Research Article
Experimental and Translational Hepatology

JOURNAL
OF HEPATOLOGY

Polyploidisation pleiotropically buffers ageing in hepatocytes

Authors

Kelvin Yin, Maren Büttner, Ioannis K. Deligiannis, …, Fabian Theis, Duncan T. Odom, Celia P. Martinez-Jimenez

Correspondence

fabian.theis@helmholtz-munich.de (F. Theis), d.odom@dkfz-heidelberg.de (D.T. Odom), celia.martinez@helmholtz-munich.de (C.P. Martinez-Jimenez).

Graphical abstract

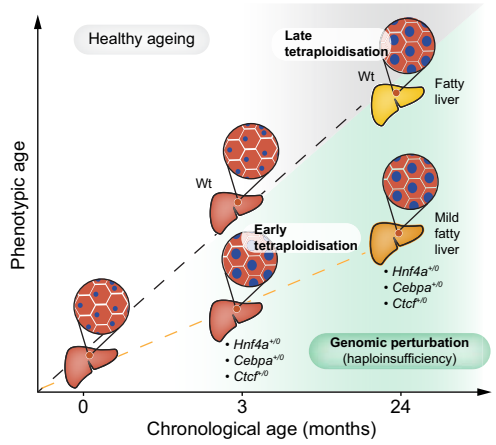

- In hepatocytes, an increase in nuclear ploidy is a fundamental cellular state that preserves tissue function
- Tetraploid hepatocyte nuclei, carrying multiple copies of the genome, attenuate age related transcriptomic changes
- Early accumulation of tetraploid nuclei in hepatocytes reduces age-related steatosis
- The impact of gene haploinsufficiencyis modulated in tetraploid hepatocyte nuclei
- The protective phenotype from polyploidisation relies on non-random selection of wild-type alleles during ageing

Highlights

- In hepatocytes, an increase in nuclear ploidy is a fundamental cellular state that preserves tissue function.
- Tetraploid hepatocyte nuclei, carrying multiple copies of the genome, attenuate age-related transcriptomic changes.
- Early accumulation of tetraploid nuclei in hepatocytes reduces age-related steatosis.
- The impact of gene haploinsufficiency is modulated in tetraploid hepatocyte nuclei.
- The protective phenotype from polyploidisation relies on non-random selection of wild-type alleles during ageing.

Impact and implications

The functional role of hepatocyte polyploidisation during ageing is poorly understood. Using single-nucleus RNA sequencing and BaseScope approaches, we have studied ploidy dynamics during ageing in murine livers with non-deleterious genetic perturbations. We have identified that hepatocytes present different cellular states and the ability to buffer ageing-associated dysfunctions. Tetraploid nuclei exhibit robust transcriptional networks and are better adapted to genomically overcome perturbations. Novel therapeutic interventions aimed at attenuating age-related changes in tissue function could be exploited by manipulation of ploidy dynamics during chronic liver conditions.

https://doi.org/10.1016/j.jhep.2024.03.043
 J. Hepatol. 2024, 81, 289–302

Research Article
Experimental and Translational Hepatology

JOURNAL
OF HEPATOLOGY

Polyploidisation pleiotropically buffers ageing in hepatocytes

Kelvin Yin[1,†], **Maren Büttner**[2,†], Ioannis K. Deligiannis[1], Mateusz Strzelecki[1], Liwei Zhang[1], Carlos Talavera-López[3], Fabian Theis[2,4,5,*], Duncan T. Odom[6,7,*], Celia P. Martinez-Jimenez[1,8,9,*]

Journal of Hepatology **2024**. vol. 81 | 289–302

Background & Aims: Polyploidy in hepatocytes has been proposed as a genetic mechanism to buffer against transcriptional dysregulation. Here, we aim to demonstrate the role of polyploidy in modulating gene regulatory networks in hepatocytes during ageing.

Methods: We performed single-nucleus RNA sequencing in hepatocyte nuclei of different ploidy levels isolated from young and old wild-type mice. Changes in the gene expression and regulatory network were compared to three independent strains that were haploinsufficient for HNF4A, CEBPA or CTCF, representing non-deleterious perturbations. Phenotypic characteristics of the liver section were additionally evaluated histologically, whereas the genomic allele composition of hepatocytes was analysed by BaseScope.

Results: We observed that ageing in wild-type mice results in nuclei polyploidy and a marked increase in steatosis. Haploinsufficiency of liver-specific master regulators (HFN4A or CEBPA) results in the enrichment of hepatocytes with tetraploid nuclei at a young age, affecting the genomic regulatory network, and dramatically suppressing ageing-related steatosis tissue wide. Notably, these phenotypes are not the result of subtle disruption to liver-specific transcriptional networks, since haploinsufficiency in the CTCF insulator protein resulted in the same phenotype. Further quantification of genotypes of tetraploid hepatocytes in young and old HFN4A-haploinsufficient mice revealed that during ageing, tetraploid hepatocytes lead to the selection of wild-type alleles, restoring non-deleterious genetic perturbations.

Conclusions: Our results suggest a model whereby polyploidisation leads to fundamentally different cell states. Polyploid conversion enables pleiotropic buffering against age-related decline via non-random allelic segregation to restore a wild-type genome.

Introduction

Liver hepatocytes are among the few human cells that are not obligatory diploid, and most often maintain multiple copies of their genome via a process known as polyploidisation. The level of polyploidisation changes during ageing and chronic liver diseases.[1,2]

To date, four main concepts, some of which are contradictory, have been proposed for how polyploidisation can shape hepatocyte and liver function during homeostasis, ageing and disease.

First, increased hepatocyte ploidy has been proposed as a pathological feature in fatty liver disease[3] and as a risk factor for developing hepatocellular carcinoma associated with a poor prognosis.[3–6] Second, polyploidisation may drive enhanced regenerative potential in chronically injured livers[7–9] and tumour protective functions.[10–12] Third, hepatocyte polyploidy might be a source of genetic diversity.[7,9,13] Fourth, having multiple genome copies might confer a versatile genomic configuration for both faithful chromosome segregation[7] and non-random selection of chromosomes to repair haploinsufficiencies under acute liver injury conditions.[8]

Polyploidisation begins during young adulthood,[14] while the hepatocyte regulatory network is also undergoing expansion and elaboration.[15–19] Hepatocyte-enriched transcription factors, including HNF4A and CEBPA, have long been studied as examples of cell type-specific master regulators, controlling lipid metabolism[20,21] and gluconeogenesis, respectively.[22] Although whole-body *Hnf4a* and *Cebpa* knockout causes embryonic[15] or neonatal lethality,[22] haploinsufficient mice are fully viable, but exhibit metabolic perturbations in multiple tissues.[23–27] Lipid homeostasis further requires the insulator protein CTCF. While homozygous deletion of *Ctcf* is embryonically lethal,[28] liver-specific *Ctcf* knockout leads to widespread steatosis.[29] In

Keywords: Liver; polyploidy; ageing; single-nucleus RNA-seq; haploinsufficiency; BaseScope; epigenetic clock.
Received 5 May 2023; received in revised form 18 March 2024; accepted 19 March 2024; available online 5 April 2024
* Co-corresponding authors.
E-mail addresses: fabian.theis@helmholtz-munich.de (F. Theis), d.odom@dkfz-heidelberg.de (D.T. Odom), celia.martinez@helmholtz-munich.de (C.P. Martinez-Jimenez).
† Co-first authors, equal contribution.
https://doi.org/10.1016/j.jhep.2024.03.043

contrast, CTCF haploinsufficiency is viable and associated with modest transcriptional perturbations on genomic CTCF occupancy[30] and CpG methylation sites.[30,31]

Here, we report that multiple independent transcriptional and genomic perturbations appear to accelerate polyploidisation in hepatocytes. This early polyploidisation ameliorates age-related lipid accumulation and maintains liver homeostasis. Finally, we present evidence that polyploid hepatocytes can employ non-random selection of wild-type alleles as a novel countermeasure to rectify genetic lesions, thus enriching for fully wild-type nuclei in aged livers.

Materials and methods

Experimental methods

Mouse models

Wild-type C57BL/6J were purchased from Charles River. To generate independent *Hnf4a, Cebpa* and *Ctcf* heterozygous knockout strains, mice with targeted alleles from The Jackson Laboratory (Hnf4a stock number: 004665; Cebpa stock number: 006230; Ctcf stock number: 022072) were purchased. Male *Hnf4a*$^{flox/flox}$, *Cebpa*$^{flox/flox}$ and *Ctcf*$^{flox/flox}$ mice were crossed with *Pgk-Cre*-positive females resulting in hemizygous offspring (*Hnf4a*$^{+/0}$, *Cebpa*$^{+/0}$ and *Ctcf*$^{+/0}$). All hemizygous mice were maintained on a C57BL/6J background by crossing male hemizygous mice with C57BL/6J females.

Mice and liver tissue collection

At the time of tissue collection, all mice were sacrificed by an approved scientist in accordance with Schedule 1 of the Animals (Scientific Procedures) Act 1986. The liver was removed from the body cavity, followed by removal of the gall bladder. One piece of liver tissue from the caudate, left lateral and right medial lobes were dissected and fixed in 10% neutral-buffered formalin solution. The remaining liver was immediately snap frozen in liquid nitrogen, then transferred to -80 °C for long-term storage.

All young mice used in this study were 3 months old. For the ageing cohort, wild-type mice were 24 months; *Hnf4a*$^{+/0}$, *Cebpa*$^{+/0}$ were 23 months; and *Ctcf*$^{+/0}$ were 20 months.

Single-nucleus isolation/homogenisation

Single nuclei were isolated as described in Strzelecki *et al*.[72] In brief, small pieces of fresh frozen liver tissue (total ±3 mm^3) was homogenised in 1 ml of homogenisation buffer (HB) (250 mM sucrose, 25 mM KCl, 5 mM $MgCl_2$, 10 mM Tris buffer, 1 μM DTT) supplemented with 1 × protease inhibitor tablet (Sigma Aldrich), 0.4 U/μl RNaseIn (Thermo Fisher Scientific), 0.2 U/μl Superasin (Thermo Fisher Scientific), 0.1% Triton X-100 (v/v) and 10 μg/ml Hoechst 33342 (Thermo Fisher Scientific) in RNase-free water. Further homogenisation was performed using a 2 ml Dounce homogeniser (Lab Logistics, #9651632) in a final volume of 2 ml ice cold HB. The liver suspension was passed through a 50 μm sterilised filter (CellTrics, Sysmex, #04-004-2327) into two pre-chilled Eppendorf tubes. Subsequently, the suspension was centrifuged at 1,000 × *g* for 8 min at 4 °C. Following centrifugation, the supernatant was removed and the nuclei pellet was resuspended in 250 μl of pre-chilled HB. To obtain high quality of single-nucleus suspensions, we performed a density gradient centrifugation clean-up procedure using Iodixanol gradient (Sigma Aldrich, Optiprep, D155). The final pellet was resuspended in 200 μl of nuclei storage buffer (166.5 mM sucrose, 5 mM $MgCl_2$, 10 mM Tris buffer pH 8.0) supplemented with additional RNase inhibitors 0.2 U/μl Superasin (Thermo Fisher Scientific, #AM2696) and 0.4 U/μl Recombinant RNase Inhibitor (Takara Clontech #2313A). Final nuclei suspension was filtered through a 35 μm cell strainer cap into a pre-chilled FACS tube prior to sorting.

Flow cytometry

Flow cytometric gating and sorting strategy was previously described in Strzelecki *et al.*[72] Briefly, Hoechst dye was used to stain all nuclei during nuclei isolation, allowing to distinguish between diploid and tetraploid nuclei using a FACS sorter (BD FACSAria IIu Cell sorter) with a 100 μm nozzle. Before sorting, 384-well thin-walled PCR plates (BioRad, #HSP3901) were freshly prepared with 940 nl of Reaction Buffer (1 μl of 10x Reaction Buffer in 2.75 μl of water). Herein, this reaction buffer will be termed Lysis Buffer 1- LB1 (Takara kit SMART-Seq v4 Ultra Low input RNA) using a liquid miniaturisation robot (Mosquito HV, STP Labtech) and kept on ice. Reaction buffer was prepared following the manufacturer instruction adding 1 μl of RNAse inhibitor in 19 μl of 10x lysis buffer. During sorting, single-nucleus suspensions were kept in nuclei storage buffer (166.5 mM sucrose, 5 mM $MgCl_2$, 10 mM Tris buffer pH 8.0) containing additional RNase inhibitors 0.2 U/μl Superasin (ThermoFisher Scientific, AM2696) and 0.14 U/μl Recombinant RNase Inhibitor (Takara Clontech, 2313A), and at concentration of ∼10x 10^4 nuclei per ml. After sorting, every plate was sealed (MicroAmp Thermo Seal lid, #AB0558), shortly vortexed (10 s), centrifuged (pre-chilled at 4 °C, 2,000xg for 1 min), frozen on dry ice and stored at -80 °C, until cDNA synthesis. All flow cytometric data were analysed by FlowJo software (Becton Dickinson & Company, version 10.7.1).

Ploidy-specific hepatocyte isolation for snRNAseq2: "double sorting strategy"

Mice were sacrificed and dissected to reveal the inferior vena cava. To perfuse and dissociate murine liver enzymatically, we followed a modified protocol based on manufacturer's methodology (Liver Perfusion Kit, Miltenyi Biotec). Briefly, a 25G butterfly-winged needle (Wing-Flo, Mediquick) was firstly inserted into the inferior vena cava without piercing the vein. The butterfly-winged needle was then attached to a syringe containing 30 ml of 1x Buffer P for perfusion over a duration of 3 min. The small caudal vein was cut to allow outflow in the first 10 s of perfusion. Immediately after perfusion, the liver was perfused with 8 ml of 1x Buffer P with Reagent C in a duration of 2.5 min. This was followed by perfusion with 9 ml of 1x Buffer P containing Reagent C, 110 μl Enzyme D, 110 μl Enzyme R and 30 μl Enzyme A in a duration of 5 min. The perfused liver was further mechanically dissociated by gently mincing with a flat-headed tweezer for no more than 5 min on a petri dish. The dissociation processed was stopped by quenching with 5 ml ice cold DMEM/10% FCS. The dissociated liver suspension was transferred into a falcon and topped up to 20 ml total volume with DMEM/10% FCS. The liver suspension was centrifuged at 50xg for 5 min at 4 °C. The supernatant was aspirated, leaving behind precipitated hepatocytes. The hepatocyte suspension was then topped to 1 ml total volume with DMEM/10% FCS and incubated with Reserpine (5 mM, 50-55-

5, ThermoFisher Scientific) at 1:1,000 dilution for 1 min at room temperature. The hepatocyte suspension was then stained with Fc receptor blocker (anti-mouse, Biolegend 101301) for 4 min, followed by staining with anti-CD31-PE (1:100, ThermoFisher Scientific, 12-0311-82), anti-CD45-PE (1:100, ThermoFisher Scientific, 12-0451-82) and Hoechst (1:1,000, ThermoFisher Scientific, H3570) for 15 min at 4 °C. The hepatocyte suspension was washed with 2 ml DMEM/10% FCS before passing through a 70 μm filter for sorting on FACS sorter (BD FACSAria IIu Cell sorter) with a 100 μm nozzle.

PE-negative and Hoechst-positive diploid, tetraploid and octaploid hepatocytes were sorted directly into PBS/10% FCS. Sorted hepatocytes were pelleted by centrifuging at 500xg for 5 min at 4 °C. The cell pallete was resuspended in 0.5 ml HB (250 mM sucrose, 25 mM KCl, 5 mM $MgCl_2$, 10 mM Tris buffer, 1 μM DTT) supplemented with 1 × protease inhibitor tablet (Sigma Aldrich), 0.4 U/μl RNaseIn (Thermo Fisher Scientific), 0.2 U/μl Superasin (Thermo Fisher Scientific), 0.1% Triton X-100 (v/v) and 10 μg/ml Hoechst 33342 (Thermo Fisher Scientific) in RNase-free water. The sorted cell suspension was transferred into a douncer and dounced 5 times using pestle B to isolate nuclei. The nuclei suspension was passed through a 35 μm filter and sorted as single -diploid, -tetraploid or -octaploid nucleus/well into 348-well plate containing snRNAseq2 chemistry.

snRNAseq2 pipeline

For generating full-length cDNA using the Smart-seq2 chemistry from a commercial kit (SMART-Seq v4 Ultra Low input RNA, Takara), we followed methodology previously described in Richter *et al.*[35] Briefly, we miniaturised the volumes by four-fold whilst keeping the same ratios for all reagents using the Mosquito HV low volume liquid handling robot (STP Labtech). Using Mosquito HV, we prepared in each well of a 384-well plate with 2,190 nl of modified snRNAseq2 lysis mix together with the first strand synthesis primers and the spike-in controls (ERCC). Ratios to the final volume (3.125 μl) of the total Lysis Buffer (1 and 2) are shown in parentheses (NP40 2% (2.5/12.5, Triton-X100 1% (1.25/12.5), ERCC spike-–in at 1/300.000 dilution (1/12.5) and 3′ SMART-seq CDS Primer II A (2/12.5) and additional water (2/12.5). Then, the plate was sealed, vortexed vigorously (20 s in a Mixmate (Eppendorf) 2000 rpm), centrifuged (30 s in a pre-chilled Eppendorf 5430R at 4 °C, 2,000 × *g*), and placed in a Thermal cycler (BioRad C1000) for 6 min at 72 °C). ERCC spike-ins were diluted 1 in 10, in water with 0.4 U/μl Recombinant RNase Inhibitor (Takara Clontech #2313A), aliquoted, and stored at –80 °C. Final ERCC dilution of 1 in 300 000 was prepared immediately before the first strand synthesis.

Next, reverse transcription and Pre-PCR amplification steps were followed as described by the manufacturer. We maintained our four-times reduced volumes for all steps. As a final modification on the Takara kit protocol, we optimised the PCR cycles program for the cDNA amplification. PCR program follows: 1 min at 95 °C, [20 s at 95 °C, 4 min at 58 °C, 6 min at 68 °C] × 5, [20 s at 95 °C, 30 s at 64 °C, 6 min at 68 °C] × 9, [30 s at 95 °C, 30 s at 64 °C, 7 min at 68 °C] × 7, 10 min at 72 °C.

Internal ERCC spike-ins were used as positive controls and the cDNA yield was assessed in an Agilent Bioanalyzer with a High Sensitivity DNA kit. In our protocol, we did not perform a bead clean-up before final library preparation. All details regarding the miniaturisation, Mosquito programmes, buffer composition, RNA-seq library preparation and sequencing can be found in previously published by Richter *et al.*[35]

RNA-seq library preparation and sequencing

Sequencing libraries were prepared using the standard Illumina Nextera XT. DNA Sample Preparation kit (Illumina, #FC-131-1096) and the combination of 384 Combinatorial Dual Indexes (Illumina- Set A to D, #FC-131-2001 to FC-131-2004). Using the Mosquito liquid handling robot, the Nextera XT chemistry was miniaturised. All the final 384-pooled libraries were sequenced using Illumina HiSeq4000 NGS sequencer in a paired-end—150 bases length.

Immunofluorescence & immunohistochemistry

After fixation of tissue for 24 h, samples were transferred to 70% ethanol. Tissues were embedded in paraffin, cut in 3- μm sections on poly-lysine-coated slides, deparaffinised, and rehydrated. Antigen retrieval was performed by incubating slides in either citrate (pH 6) or Tris-EDTA (pH 9) solution and heat-induced in a vegetable steamer for 30 min at pre-boiling temperature.

For immunofluorescence, sections were permeabilised in 0.25-0.5% Triton X-100, then blocked with 3% donkey serum for 30min. All antibodies were prepared in antibody diluent buffer: 0.1% (v/v) Tween in PBS containing 300 mM NaCl. Sections were incubated with primary antibody: rabbit anti-b-catenin (Cell Signalling, D10A8, 1:50), rabbit anti-pH2AX (Cell Signaling, Ser139, 1:400), rabbit anti-Ki67 (Abcam, 15580, 1:1000) overnight at 4 °C. Sections were washed and stained with secondary antibody: donkey anti-rabbit Alexa Fluor 555 (ThermoFisher Scientific, A32794, 1:800), and nuclei stain 4',6-diamidino-2-phenylindole (DAPI; ThermoFisher Scientific, Cat No. 62248, 1:1,000) for 2h at RT. Additionally, apoptosis visualisation was performed using the commercial TUNEL immunofluorescence staining kit (Roche, 11684795910) following manufacturer's instructions. Sections were washed with antibody diluent buffer and mounted with VectaShield mounting media (Vectorlabs). All incubations were performed in dark and humidified chambers.

For immunohistochemistry, counterstaining of nuclei with haematoxylin and eosin (abcam, ab245880), as well as staining of fibrotic tissues with Picro Sirius Red staining (Abcam, ab150681) were performed following manufacturer's protocol.

BaseScope and nuclei genotype scoring

BaseScope probes were custom designed with Advanced Cell Diagnostics. Pair probes: BA-Mm-Hnf4a-tv1-E4E5-C1 (Ref: 1141091-C1, Lot: 22046A, sequence: CTGTCCAAAATGAGCGGGACCGGATCAGCACGCGGAGGTCAAGCTACGAGGACAGCAGCCTGCCCTCCATCAACGCGCTCCTGCAGGCAGAGGTTCTGTC CCAGCAGATCACCTCTCCCATCTCTGGGATCAATGGCGACATTCGGGCAAAGAAGATTGCCAACATCACAGACGTGTGTGAGTCTATGAAGGAGCAGCTG CTGGTCCTGGTCGAGTGGGCCAAGTACATCCCGGCCTTCTGCGAACTCCTTCTGGATGACCAG) and BA-Mm-Hnf4a-tv1-E3E6-C2 (Ref: 1141101-C2, Lot: 22045A, sequence: GTTTAGCCGACAATGTGTGGTAGACAAAGATAAGAGGAACCAGTGTCGTTACTGCAGGCTTAAGAAGTGCTTCCGGGCTGGCATGAAGAAGGAAGGT GGC GCTGCTCAGGGCCCACGCCGGTGAGCATCTGCTGCTTGGAGCCACCAAGAGGTCCATGGTGTTTAAGGACGTGCTGCTCCTAG). BaseScope assays were performed in accordance

with guidelines provided by the manufacturer (Advanced Cell Diagnostics, Newark, CA). Briefly, paraffin sections of 5 μm thickness on Superfrost plus slides were deparaffinised in xylene (2 × 5 min) and ethanol (2 × 5 min), then dried at 60 °C for 2 min. Sections were then incubated in hydrogen peroxide 10 min at RT, followed by target retrieval for 30 min at 100 °C, then incubated in protease for 30 min at 40 °C, with rinsing with distilled water between treatments. BaseScope probes were applied for 2 h at 40 °C in a HybEZ oven before incubation with reagents following the sequence: AMP1 (30 min at 40 °C), AMP2 (30 min at 40 °C), AMP3 (15 min at 40 °C), AMP4 (30 min at 40 °C), AMP5 (30 min at 40 °C), AMP6 (15 min at 40 °C), AMP7 (1 h at RT), AMP8 (15 min at RT), Duplex-Fast Red (10 min at RT), AMP9 (15 min at 40 °C), AMP10 (15 min at 40 °C), AMP11 (1 h at RT), AMP12 (15 min at RT), Duplex-Green (10 min at RT). Slides were subsequently counterstained with 50% hematoxylin solution for 90 sec before dried at 60 °C for 15 min, followed by mounting in VectaMount antifade solution (Vector labs, Burlingame, CA). BaseScope images were acquired from Leica upright brightfield microscope with either HI PLAN 1 20x/0.30 PH1 or HI PLAN 1 40x/0.50 PH1 lens on a DMC4500 camera.

For each nucleus, the total number of green (wild-type) or red (excised *Hnf4a* exon) signals were counted. A combined total number of signals were then calculated and categorised as either diploid or tetraploid nuclei, where the number of signals equals 2 or 4, respectively. Importantly, nuclei containing 3 or more than 5 signals were discarded for downstream analyses. Nuclei containing only green or red signals were scored as wild-type or knockout, respectively. Nuclei containing equal ratio of green and red signals were scored as hemizygous. All nuclei were counted by eye on immunohistochemistry images taken with a 40x magnification lens.

Microscopic imaging and analyses

Fluorescence images were obtained using the Zeiss 880 upright laser scanning confocal microscope with either 20x/1.0NA W Plan-Apochromat DIC or 63x/1.2NA W Korr C-Apochromat lens. Z stack of approximately 10 μm thickness was imaged. Z stack with maximum projection was later generated using the Fiji/Image J software (version 2.3.0/1.53f). Histological sections were scanned using an Axio Scan 7 with an AxioCam 705 colour 14-bit colour camera. Pictures were taken with 20x/0.8NA Plan-Apochromat M27 and 40x/0.95NA Plan-Apochromat M27 objectives. All scanned images were visualised with ZEISS netScope viewer.

Fiji/Image J software (version 2.3.0/1.53f) was used to measure areas (μm^2) of each visibly distinct nuclei with circularity of at least 0.7, DAPI images were processed using a 'Otsu' filter, followed by Smooth Edge' and 'Watershed' algorithms in Fiji software. Measurements of nuclei area were then converted to diameter in order to extrapolate and score nuclei as 2n, 4n or >8n ploidy as described in Richter *et al.*[35] Morphometric analysis of lipid content to quantify liver steatosis was performed as described in Finan *et al.*[33]

Imaging analyses for cellular and nuclei ploidy

Scanned liver sections were visualised in Visiopharm software. Briefly, pericentral and periportal zones of interest were annotated according to presence of entire liver sections were annotated for pericentral and periportal zonal regions were annotated based on the absence or presence of portal triade, respectively. Each region of interest was subjected to Deep Learning based application for nuclei detection in the image analysis software Visiopharm (Version 2023.09.01 4530 Visiopharm, Hoersholm, Denmark). Thereby, each hepatocyte was scored as either mononuclear or binuclear cells. Nuclear area was also calculated to distinguish ploidy levels as diploid, tetraploid or octoploid.

Epigenetic clock using the Mouse Methylation BeadChip

Healthy mice of young and old age from each strain were selected for DNA methylation analysis. DNA from frozen liver tissue was extracted using the DNeasy Blood and Tissue Kit (Quiagen), following the manufacturer's protocol. In total 48 tissues were analysed using the Infinium Mouse Methylation BeadChip (Illumina, San Diego,USA) as detailed before in Fennell *et al.* (Fennell *et al.*, 2022, Cell Reports Methods). In short, normalised DNA was bisulfite converted, amplified, then fragmented and purified before hybridisation on the BeadChip. The arrays were performed by the Genomics core facility in HMGU.

Software

GraphPad Prism Version 8.4.3 (471) was used to analyse and visualise data. Adobe Illustrator Version 25.0.1 was used to construct all figures.

Computational methods

Read alignment and preprocessing

Raw sequencing reads were mapped against a customised genome containing both mm10 (GRCm38, assembly version 93), and the ERCC92 sequences. Mapping was done using Spliced Transcripts Alignment to a Reference (STAR) software (version 2.7.1a) with the following parameters –outFilterMultimapNmax 1 –outSAMtype BAM SortedByCoordinate. Potential PCR duplicates were identified and removed using MarkDuplicates from picard tools version 2.20.2 with the option REMOVE_DUPLICATES=true. For every single nucleus, reads mapping to individual transcripts were counted and summed per gene using htseq-count version 0.11.3 with the following parameters: -m intersection-nonempty -f bam -r pos -s no –nonunique all -t transcript -i gene_id –additional-attr=gene_name.

The resulting raw count matrix was loaded into python and stored as an AnnData object, anndata version 0.7.1. The downstream analysis described below was adapted from Luecken *et al.* Unless described otherwise, functions implemented in scanpy (version 1.4.5.2.dev6+gfa408dc7) were used in downstream analysis. Additionally, to the count matrix based on full transcripts, count matrices for exonic and intronic reads, respectively, were built using featureCounts.

Quality control and filtering

For each cell, we computed the fraction of ERCC reads as the number of reads aligned to ERCC spike-in genes divided by the total number of reads per cell. Cells with less than 5% and more than 90%, respectively, were filtered out. Next, we removed all cells with less than 200 genes and more than 7,000 genes expressed, respectively. We further excluded all cells with more than 300,000 reads. As a low count filter, we used 2,500 for the aged group samples and 3,500 for the young

group samples. Lastly, all cells with unknown ploidy state were removed. Then, we excluded two plates with technical replicates and two plates with overall low quality. After normalisation, we removed all cells with a total gene length-corrected read count higher than 60,000. The final dataset consists of 6,605 cells expressing 30,520 genes.

ERCC size factor calculation and normalisation

As described previously in Richter *et al.*,[35] we compute an ERCC size factor based on the number of reads aligned to ERCC spike-in genes divided by the mean detection level of ERCC spike-ins and multiplied by 10,000. As the SMART-Seq2 protocol allows to capture reads from the entire length of the gene body, we correct the reads by gene length, *i.e.* the number of reads per gene in a cell is divided by the length of the gene model and multiplied by 1,000. Using the ERCC size factor, we derive a cell specific normalisation factor (RPK factor) as the total gene length-corrected read count divided by the ERCC size factor. The final transcripts per million (TPM) normalisation is the gene length-corrected read count divided by the RPK factor. The TPM normalised data is then log-transformed with a pseudocount of 1. We account for batch effect with ComBat. All analyses are carried out in scanpy v.1.5.1 in Python v.3.8.

Data visualisation and clustering

High dimensionality of the normalised expression matrix was reduced by calculating the first 50 principal components. Data points were embedded using t-distributed stochastic neighbourhood embedding (t-SNE) based on the first 10 principal components and a perplexity of 50. After removing hepatocytes from the count matrix, *Louvain* clustering with a resolution of 0.2 was used on the neighbourhood graph was used to separate the cluster of non-parenchymal annotation.

To visualise changes of gene expression and distribution, genes with zero expression across cells were removed as well as cells that did not express any genes. The number of genes per cell and expression levels were visualised in violin and dot plots throughout the manuscript. Visualisations were created using scanpy v.1.6.0.

Analysis of cellular and nuclear ploidy using snRNAseq2 and a "double sorting strategy"

Data acquisition and preprocessing: Paired-end RNA sequencing data were aligned using STAR-2.7.1a, a commonly used tool for aligning high-throughput RNA-seq data. A pre-built STAR index, generated from a reference genome with appended spike-in sequences (ERCC92), served as the genomic scaffold for the alignment. Following the alignment process, each sample's resulting BAM files were sorted by genomic coordinates and available for downstream analysis. PCR duplicates resulting from library preparation and sequencing were identified and removed from the aligned BAM files using the Picard tools suite (version: 3.1.1). Picard MarkDuplicates was employed for its efficacy in pinpointing and flagging duplicate reads. For gene expression quantification, we used the htseq-count tool from the HTSeq framework (version: 0.11.3). Gene expression levels were quantified in terms of read counts mapped to each gene. The output was a matrix of raw read counts, which could be used for subsequent normalisation and differential expression analysis. By encompassing ERCC spike-ins within the quantification process, we incorporated a control for technical variability which could be used to assess data quality and normalisation efficiency in downstream analyses.

System and Package Configuration: R (version 4.0.3; R Core Team, 2020) and RStudio were used for all analyses. Packages required for single-cell RNA-seq (scRNA-seq) data analysis, including Seurat, Signac, dplyr, and others, were installed from CRAN and Bioconductor repositories. Libraries specific to mouse genome annotation such as EnsDb.Mmusculus.v79 and org.Mm.eg.db were installed from AnnotationHub. Parallel processing was enabled using the future and future.apply packages to maximize computational efficiency. The Seurat object assay version was set to 'v4' to ensure compatibility with subsequent analyses.

scRNA processing and visualisation: The scRNA-seq count matrix was acquired from HTSeq-count and imported into R. Genome annotation files were processed to create a metadata frame for genes, including gene names, sources, and biotypes. Then, quality control was performed to ensure matching between raw count gene IDs and gene IDs in the genome annotation file, including spike-in ERCC controls. This step was critical in distinguishing endogenous genes from spike-ins later in the analysis. Transcript lengths for genes were computed using the annotation file, and TPM (Transcripts Per Million) normalisation was conducted to accommodate differences in gene length and sequencing depth across samples. ERCC spike-in controls were used to calculate the proportion of ERCC in each cell, which served as a metric for technical variation. Cells with extreme values for gene counts, total counts, percentage of ERCC, or complexity were filtered out to ensure the quality of downstream analyses. A Seurat object was created, incorporating the TPM-normalised count data, relevant quality control metrics, and metadata. Additional metadata, such as ploidy status and age, were factored in for subgroup analyses. The Seurat object was processed, including identification of variable features, scaling, and regression of unwanted sources of variation (*e.g.*, total counts, percentage ERCC). Principal component analysis (PCA) was conducted to reduce data dimensionality. With the selected principal components, nearest neighbour graph construction and subsequent clustering were performed to identify distinct cell populations within the dataset. Both UMAP (uniform manifold approximation and projection) and t-SNE were applied for non-linear dimensionality reduction to visualise clusters. Cell populations were characterised and visualised based on metadata such as ploidy status and age.

Inter-cluster similarity analysis: Jaccard correlation heatmaps were generated to examine the similarity between cell populations grouped by ploidy status. A combination of different resolutions and features were tested to achieve the most informative correlation patterns.

Cell cycle analysis and inter-cell type correlation

Cell cycle states were established using *cyclone* as implemented in the scran R package. All nuclei were classified into G1, S or G2M phase based on their normalised gene counts. Analysis was carried out per strain.

Gene ontology analysis
Python package *gprofiler* was used to visualise genes enriched in functionally relevant groups, focusing on the ontology *biological process.*

Transcriptional variability
Log-transformed mean expression of genes expressing less than 0.25 were removed for calculation due to that fact that lowly expressed genes have higher transcriptional variability. *Co-efficient of variation* was calculated on the normalised log-transformed and batch-corrected matrix by making use of the formula described in Canchola *et al.*[73] Mann-Whitney *U* tests were performed to detect significance between different ages across all different cell types, as well as 2n and 4n ploidy hepatocytes.

Pseudotermporal ordering
Non-parenchymal nuclei were removed from the matrix and zonation markers were obtained from Halpern *et al.*[74] Principle components and t-SNE were re-calculated based on this count matrix of nuclei with zonation marker genes. Nuclei were ordered along the zonation gradient using diffusion pseudotime.[75] Outliers with a DPT 0.42 were removed. Based on marker gene expression and *Louvain* clustering (resolution = 0.7), nuclei were clustered into groups designated by pericentral, periportal or non-zonated marker genes. The percentage of diploid and tetraploid nuclei was calculated for each cluster and expressed as bar plots.

Differential expression analysis
Two-sided Welch's t-tests were performed as implemented in the scanpy function *rank_genes_groups*. This was done by comparing different age groups, strains and ploidy of hepatocytes. Genes that had a $\log_2$ fold change smaller larger than 0.5 and a Benjamin-Hochberg-adjusted *p* value below 0.05 were considered significantly upregulated; genes with a $\log_2$ fold change smaller than -0.5 and a Benjamin-Hochberg adjusted *p* value below 0.05 were considered significantly downregulated.

To further investigate changes in the distribution of a given gene between hepatocytes of different ploidy or different age, a Kolmogorov–Smirnov test was performed. Genes were called as significantly changing their gene expression distribution if they had a *p* value below 0.05 and a test statistic of >0.15.

A more stringent filtering strategy was then applied to obtain biologically relevant DEGs in hepatocytes when comparing ploidy or different age. Briefly, only genes expressed in less than 15 nuclei; gene names beginning with *Gm* or ending with *Rik*; *p* value >0.5; log2FC <0.5; and mean expression value <1, were disregarded. Resulting genes after the stringent filter were used for comparison using a Venn diagram.

Co-expression fraction analysis
To construct arc plots, the R package *arcdiagram* was used. Briefly, six classes of genes grouped by KEGG terms were selected. Each class of genes were coloured with mean expression of individual genes represented as the size of dots. A co-expression fraction score for each gene was determined using normalised mutual information, in which a range of 0 (no mutual information) to 1 (perfect overlap) was determined. Here, genes with a positive expression level were considered expressed. Subsequently, scores of less than 0.7 were filtered out for the final visualisation of arc plot.

Epigenetic clock
Data Acquisition and System Configuration: Raw methylation data were acquired from the BeadChip platform. For data processing and statistical analysis, we utilized the R software environment (version 3.6.1). We employed several R packages including SeSAM (https://github.com/zwdzwd/SeSAM) for preprocessing the IDAT files, ggpubr for data visualisation, FactoMineR and factoextra for PCA, and future and future.apply for parallel computation to increase the efficiency of data handling. Moreover, the Bioconductor package SummarizedExperiment was used to manage the assay data. A computation plan using 16 cores in a multisession parallelized setup was established to facilitate concurrent execution of tasks during data preprocessing.

Data preprocessing and quality control (QC): The dataset was preprocessed using the SeSAM package. A custom preprocessing function included temperature, quantile colour adjustment, dye-bias, and a peak-based correction (TQCDPB). Following the initial data loading, QC steps were applied to each sample. QC was performed to assess signal quality by calculating detection *p* values and signal intensity values. We also generated quantile-quantile plots and intensity-beta value plots for each sample to further inspect and visualise data quality.

Principal component analysis (PCA): PCA was conducted on the batch-corrected beta values to capture the major sources of variation within the dataset. The PCA was executed using the FactoMineR package, retaining the first five principal components. The eigenvalues of the principal components were visualised to evaluate their contribution to the total variance. Subsequently, PCA plots were created using the factoextra package, incorporating genotype- and age-specific colouring schemes, to provide visual summaries of sample distributions in the context of age groups and genotypes.

Ageing prediction analysis: Beta values were extracted for ageing prediction analysis. The *predictMouseAgeInMonth()* function from SeSAM package was used to predict the age in months for each mouse sample based on methylation patterns. Predicted ages were then compiled into a dataset.[76]

Data integration and linear regression analysis: We merged the experimentally obtained chronological ages with the predicted ages derived from the methylation data. A linear model analysis was carried out to correlate predicted ages with chronological ages across different genotypes. We utilized ggpubr2 to visualise the results and extract information regarding the fit of the models in terms of equations and R-squared values as well as grouped boxplots.

Results

Ageing leads to an increase in hepatocyte ploidy and regulatory complexity

We first confirmed that ageing in wild-type mice causes the accumulation of hepatic fat and increased hepatocyte ploidy[32] (Figs 1A,B and S1A,B). All studied mice showed normal histological profiles, with no signs of abnormal fibrosis or apoptosis by staining of Sirius Red and TUNEL, respectively (Fig. S1). We next analysed the liver lipid content on H&E sections and

scored steatosis using a semi-quantitative grading system.[33] As expected, young livers had very little fat deposition, and aged livers had a mixture of micro- and macro-vesicles of lipids (Fig. S1B).[34]

To quantify individual nuclei of hepatocytes as diploid (2n), tetraploid (4n) or octoploid (8n), we performed immunofluorescent imaging-based analysis, which was developed in our laboratory,[35] and determined that old livers showed an enrichment of 8n nuclei in comparison to young livers (Fig. 1B). The relative proportion of 2n and 4n hepatocyte nuclei also changed in aged livers. These results were later validated by FACS analysis (Fig. S1C,D).

We identified the ploidy-related transcriptional changes occurring between young (3M) and old (24M) mice by flow-sorting 2n and 4n nuclei from wild-type mouse liver cells, followed by profiling of the nuclear transcriptome using snRNA-seq2[35] (Fig. 1C). t-SNE showed that nuclear tetraploidy was exclusively found among hepatocytes, and that ageing only modestly shifted the cell type composition in the liver (Figs 1D and S1E, Table S2)[36,37]).

By compiling the single-nucleus data into a pseudo-bulk analysis, we identified that old 2n nuclei from hepatocytes showed a larger number of downregulated genes (1,740 genes) compared with old 4n hepatocyte nuclei (1,090 genes). From old 2n and 4n hepatocyte nuclei, we found 96 genes commonly downregulated, including well-studied lipid metabolism genes such as *Acss2*, *Acly*, *Acot11*, *Nr4a3 (NOR1)*, *Slc38a7* (Fig. 1E, Table S1). We further investigated whether transcriptomic differences in 2n nuclei isolated from hepatocytes of different cellular ploidy could be found. To this end, intact hepatocytes were FACS sorted based on their cellular ploidy, followed by nuclei isolation and the downstream snRNA-seq2 pipeline (Fig. S2, and methods). *Louvain* clustering was performed to construct the neighbourhood graph, and the t-SNEs were

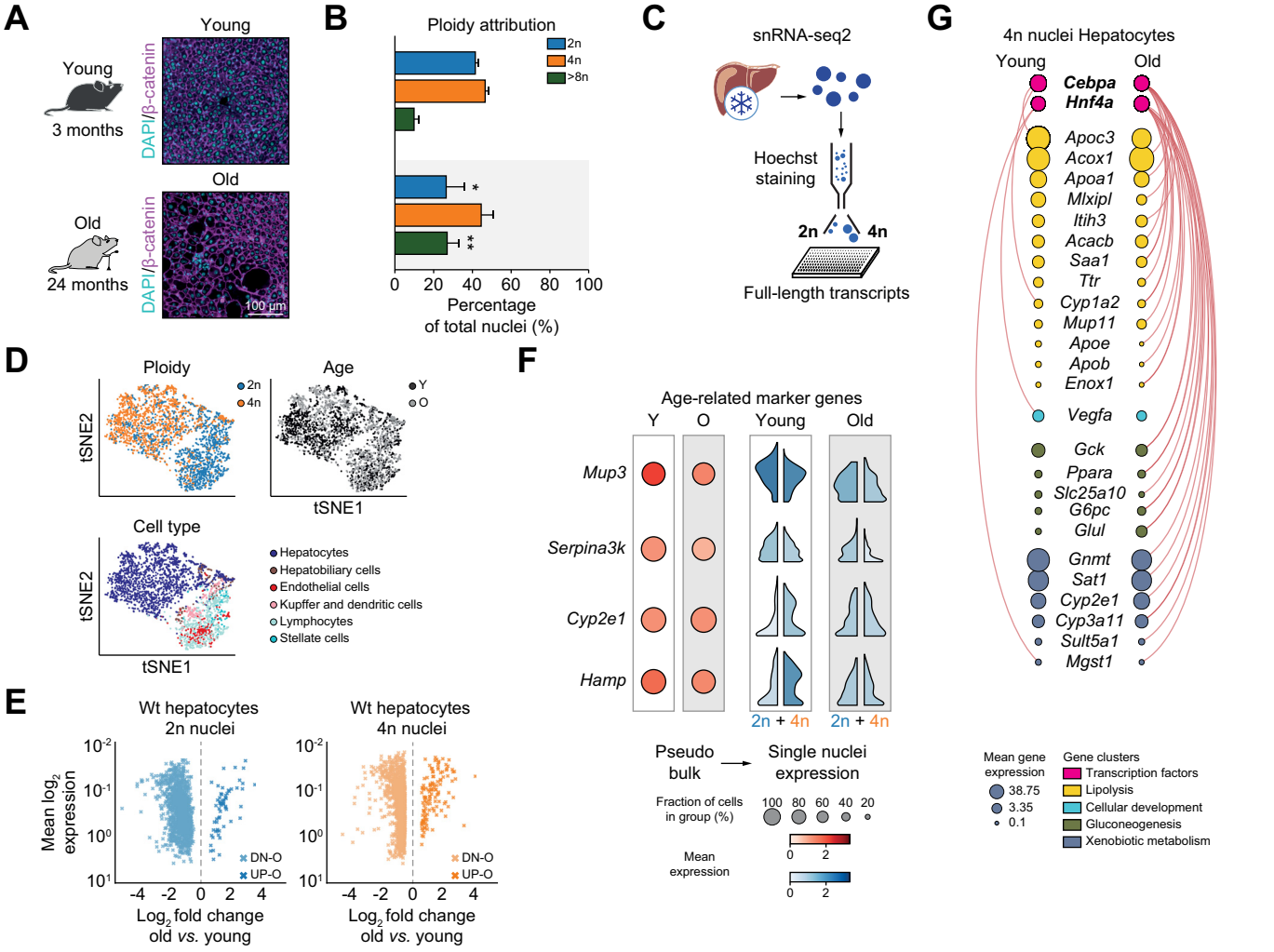

Fig. 1. Ageing increases hepatocyte ploidy and regulatory complexity. (A-B) Nuclei from WT mouse livers (young n = 6, old n = 6) were scored by ploidy level, evaluated by co-immunofluorescence staining of β-catenin and DAPI to calculate nucleus diameter. Student t-test between young and old within same ploidy levels was performed, where *, *p*-value < 0.05; **, *p*-value < 0.01; ***, *p*-value < 0.001. (C) Nuclei were isolated from frozen livers (WT young n = 4, old n = 3), ploidy determined by Hoechst staining, and sorted into plates for transcriptome analysis. (D) t-SNE annotated by ploidy, age, and cell type. (E) MA plot of transcriptional differences between young and old hepatocytes for diploid (top) and tetraploid (bottom) nuclei. (F) Expression levels of age-related markers by pseudo-bulk (left, dot plots) and single-nucleus transcriptome analyses (right, violin plots). (G) Co-expression analysis of *Hnf4a* and *Cebpa* with their direct downstream target genes in young (left) *vs.* old (right) tetraploid hepatocytes; red arcs indicate significant co-expression. DN-O, downregulated in old; t-SNE, t-distributed stochastic neighbourhood embedding; UP-O, upregulated in old; WT, wild-type.

calculated as embeddings. No sub-clusters were identified in 2n nuclei isolated from diploid or tetraploid binucleated cells, showing no transcriptomic differences between 2n nuclei (Fig. S2E). Interestingly, in these wild-type mice, analysis of transcriptional noise indicates that diploid and tetraploid hepatocyte nuclei maintain coordinated transcriptional responses during ageing (Fig. S1H).[38–41]

Our data also revealed that many previously reported marker genes attributed to ageing in hepatocytes[42–46] were instead ploidy-dependent even in young animals (Fig. 1F). For instance, *Mup3* and *Serpina3k* are downregulated during ageing, but we observed a more prominent downregulation in 4n hepatocyte nuclei; on the contrary, *Cyp2e1* and *Hamp* marker genes are upregulated during ageing, but we observed a selective upregulation in 4n young hepatocytes (Fig. 1F, Tables S1 and S3). Gene ontology analysis showed that 4n hepatocyte nuclei were enriched in fatty acid metabolic processes (Fig. S3A,B). Prior studies have correlated cellular senescence with ageing, but we did not observe ploidy-related changes in senescence markers, such as *Rela*, *Mtor*, *Cdkn1a*, *Cdkn2d*, *Rab31,* and *Trp53,* during healthy ageing (Table S1).[47] Therefore, quantification of hepatocyte ploidy is required to accurately monitor ageing through transcriptional changes of key age-related marker genes.

Finally, we asked whether ageing restructures the liver-specific regulatory networks of diploid and tetraploid hepatocytes in the context of the nuclear transcriptome.[48] Co-expression analysis of two key upstream liver-specific transcriptional factors (*Cebpa* and *Hnf4a*) in our wild-type mice showed increased robustness of the regulatory networks during ageing in 4n nuclei from hepatocytes (see Methods, Fig. 1G). This result indicates that from early development, hepatic transcription factors gradually increase their regulatory complexity across the lifespan of tetraploid hepatocytes.

Haploinsufficiency of tissue-specific master regulators increases metabolic buffering via early tetraploidisation

When subject to otherwise lethal injury, such as the deletion of *Fah* gene, polyploidy has been described as a mechanism to enhance hepatocyte survival by enabling the selection of favourable alleles[7,8,13,49]. We asked whether a similar mechanism could shape hepatocyte responses to less severe perturbations, such as haploinsufficiency of liver master regulators that are phenotypically normal. We generated two independent haploinsufficient mice, *Hnf4a*$^{+/0}$ and *Cebpa*$^{+/0}$, to precisely dissect the genome-wide effect of a single-gene copy inactivation in diploid and tetraploid hepatocytes during ageing (see Methods, Fig. 2A). *Hnf4a*$^{+/0}$ and *Cebpa*$^{+/0}$ mice showed striking reduction of liver steatosis in aged mice (Figs 2B and S4A), and early polyploidisation (Figs 2C and S4B,C). In young haploinsufficient mice, we quantified the reduction of 2n nuclei in hepatocytes and the increase in polyploid nuclei in the intact liver tissue by immunohistochemistry, and further validated the nuclear ploidy changes by FACS analysis (Fig. S4B,C). In snRNA-seq2 data of *Hnf4a*$^{+/0}$ and *Cebpa*$^{+/0}$ aged livers, we identified all major cell types with the majority of tetraploid nuclei assigned to the hepatocyte cluster using *Louvain* clustering and liver-specific marker genes (Fig. 2D,E). In aged livers from both haploinsufficient mice, we did not find major nuclear transcriptional changes despite the single-copy gene deletion of liver-enriched transcription factors (Fig. S4D,E).

Interestingly, we did observe an increase in transcriptional variability in the tetraploid nuclei from old hepatocytes in both haploinsufficient mice (Fig. S4E), suggesting that genomic perturbations might change the rate of burst initiation and the polymerase pause stability,[50–52] most likely to optimise cell function.[53] Ageing had a more prominent effect on 4n hepatocyte nuclei (Fig. 2F,H), with 123 genes and 67 genes downregulated in *Hnf4a*$^{+/0}$ and *Cebpa*$^{+/0}$ mice, respectively (Table S2). Additionally, haploinsufficiency led to differential gene expression profiles between 2n and 4n hepatocyte nuclei when considering both changes in gene expression levels and expression distributions (Fig. 2G,I, Table S2). For instance, in *Hnf4a*$^{+/0}$ mice, genes involved in lipid metabolism such as *Acox1*, *Apob*, and *Fapb1*, were upregulated in 4n nuclei from young hepatocytes, but reveal differential downregulation in 2n and 4n nuclei in old hepatocytes. Similarly, genes involved in glucose metabolism, (*e.g*. *Ttr*, *Pck1*, and *AldoB*), further showed that tetraploidisation buffered the genomic perturbation in haploinsufficient mice (Fig. 2G,I). We found similar ploidy-dependent gene expression in *Cebpa*$^{+/0}$ mice (Table S4). Thus, during ageing, hepatocyte ploidy maintains liver homeostasis in haploinsufficient mice upon single-copy gene deletion of key master regulators.

Polyploidisation in hepatocytes buffers the transcriptional impact of genetic perturbations

Hypothesising that early polyploidisation could be a universal mechanism to maintain tissue homeostasis, early polyploidisation might be a general response of hepatocytes to genotypic perturbations instead of being limited to haploinsufficiency of liver-specific master regulators. We therefore inspected the effect of knocking out one copy of CTCF, which produces very mild liver phenotypes in young mice[31]; albeit the impact of ageing has not been characterised. We created and aged *Ctcf*$^{+/0}$ haploinsufficient mice, and characterised their liver histology, ploidy, and performed snRNA-seq (Fig. 3A) (see Methods). Like the liver-enriched master regulator haploinsufficient mice, the CTCF haploinsufficient mice showed early tetraploidisation when young (Figs 3B and S5A-E). Increased nuclear ploidy was observed in young and old *Ctcf*$^{+/0}$ haploinsufficient mice and in the liver-enriched haploinsufficient mice, with no changes in cellular ploidy, cell proliferation, and DNA damage (Fig. S6). Specifically, when we performed quantification analysis of lipid droplets across the periportal-central axis (see Methods), all haploinsufficient mice showed a reduction of lipid accumulation in the pericentral zone (Fig. 3C, Table S6).

We asked whether the knockout of CTCF created a transcriptionally similar phenotype as liver-specific knockouts. By performing snRNA-seq2 followed by dimensionality reduction analysis and *Louvain* clustering, we observed no separation of the different strains in either young or old mice (Fig. 3D left); nor could we identify subpopulations based on ploidy (Fig. 3D right, Fig. S7). We then compared the gene expression profiles of the single-nucleus RNA-seq data from hepatocyte nuclei, differentiated by age and genotype, but not ploidy. To our surprise, this analysis showed that most age-related downregulated

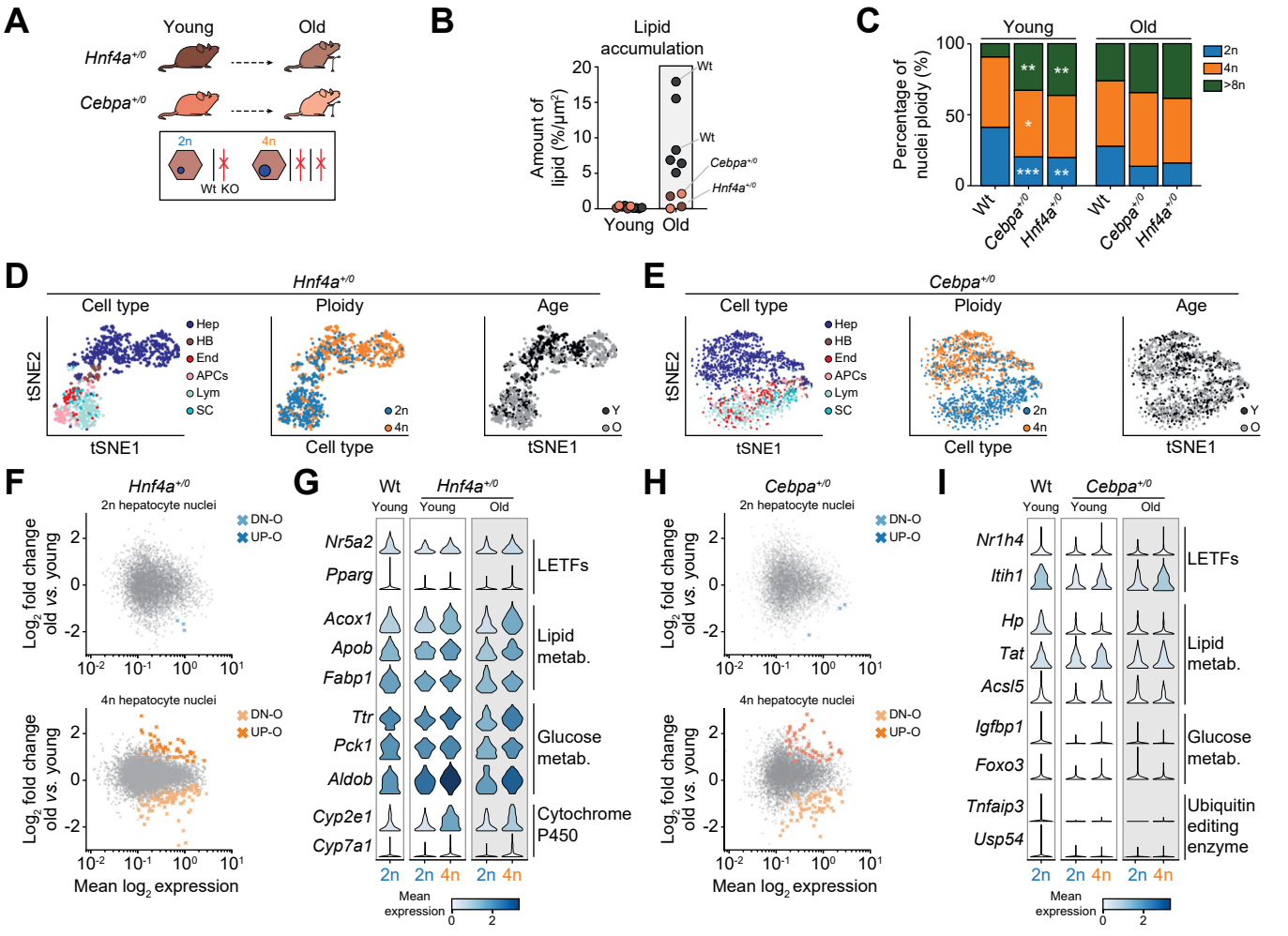

Fig. 2. Early tetraploidisation maintains liver homeostasis during ageing in *Hnf4a*$^{+/0}$ and *Cebpa*$^{+/0}$ haploinsufficient mice. (A) Young and old *Hnf4a*$^{+/0}$ and *Cebpa*$^{+/0}$ mice (young, n = 2, old, n = 2) were used to study the transcriptional and ploidy impact of master regulator haploinsufficiency. (B) Quantification of lipid accumulation in murine livers by %/µm^2; dots are biological replicates (WT: young n = 6, old n = 6; haploinsufficient mice: young n = 2, old n = 2). (C) Quantification of nuclear ploidy by image analyses shows that transcription factor haploinsufficiency causes early polyploidisation in young livers (one-way ANOVA compared to WT, where **, *p*-value < 0.01; ***, *p*-value < 0.1) . (D-E) t-SNE plot of single-nucleus RNA-seq of *Hnf4a*$^{+/0}$ and *Cebpa*$^{+/0}$ mice showing all major cell types, annotated by ploidy and age. (F) MA plot of transcriptional differences between young and old *Hnf4a*$^{+/0}$ hepatocytes for diploid (top) and tetraploid (bottom) nuclei using differential expression analysis (Methods). (G) Gene expression distribution across single nuclei of *Hnf4a* target genes are shown as violin plots, which are shaded by overall gene expression level. (H–I) MA plot as above and gene expression distribution across single nuclei for *Cebpa*$^{+/0}$ and its target genes. LETFs, liver-enriched transcription factors; RNA-seq, RNA sequencing; t-SNE, t-distributed stochastic neighbourhood embedding; WT, wild-type.

genes were highly specific to their respective regulator knockout, and only four genes were commonly downregulated during ageing (see Methods, Fig. 3E, Table S4). Similarly, we found that almost no upregulated genes in the aged cohorts were shared between knockouts, but the two shared upregulated genes in ageing, *Cyp4a14* and *Elovl5,* are central to lipid metabolism[54,55]

Interestingly, liver-specific deletion of CTCF in young mice induces dysregulation of lipid metabolism through indirect mechanisms.[29] In our *Ctcf* haploinsufficient mice, we observed differentially upregulated genes involved in lipid homeostasis in 4n nuclei isolated from hepatocytes (Figs 3F and S5F,G, Table S5), suggesting that 4n hepatocyte nuclei transcriptionally buffer lipid metabolic function in response to genetic perturbation upon *Ctcf* haploinsufficiency. Importantly, early polyploidisation is not limited to hepatocyte-specific functional mechanisms, but a conserved mechanism that ameliorates ageing-related liver steatosis.

Hepatocyte ploidy protects during ageing by non-random selection of the wild-type allele

Early polyploidisation could improve metabolic function at the transcriptional level[56,57]. Indeed, gene ontology analysis in 4n hepatocyte nuclei from haploinsufficient mice also exhibited enrichment in cellular and tissue homeostasis terms (Fig. S8). Additionally, we proposed that in response to a genetic perturbation, 4n nuclei from hepatocytes can undergo a non-random selection of the wild-type allele to support cellular homeostasis (Fig. 4A). To test this hypothesis, we first

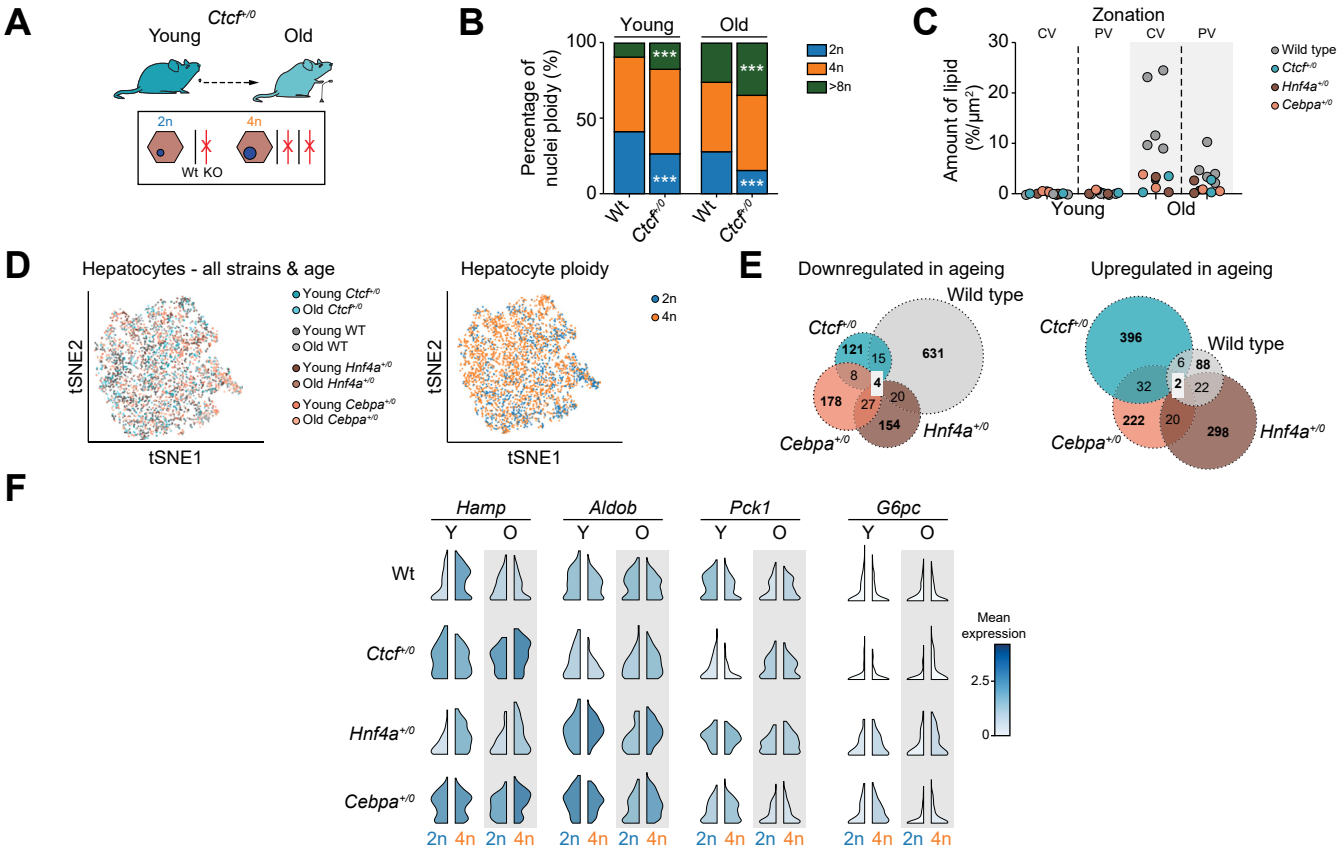

Fig. 3. Analysis of *Ctcf*$^{+/0}$ haploinsufficient mice reveals that early polyploidisation is a general mechanism to maintain liver homeostasis. (A) Analysis of young and old hepatocytes with haploinsufficiency of *Ctcf* (*Ctcf*$^{+/0}$) by ploidy (young n = 2, old n = 2). (B) Quantification of nuclear ploidy shows that *Ctcf* haploinsufficiency causes early polyploidisation in young livers (WT: young n = 6, old n = 6; haploinsufficient mice: young n = 2, old n = 2; one way ANOVA compared to WT was performed, where ***, *p*-value < 0.001) (C) Quantification of lipid accumulation in the pericentral (CV) and periportal (PV) area. (D) t-SNE plot on hepatocytes labelled by genotype and age (left) or ploidy (right). (E) Venn diagram comparing the genes downregulated (left) and upregulated (right) during ageing for all genotypes after stringent filtering was applied. (F) Gene expression in violin plots, which are shaded by overall gene expression levels, for lipid metabolic genes upregulated during ageing in *Ctcf*$^{+/0}$ compared to gene expression distribution across single nuclei, separated by ploidy. KO, knockout; t-SNE, t-distributed stochastic neighbourhood embedding; WT, wild-type.

compared the log-ratios of relative expression level between 2n nuclei from hepatocytes in wild-type against *Hnf4a*$^{+/0}$ mice showing the expected transcriptional dysregulation[15,20] (Fig. 4B). However, correlation analysis indicated that the transcriptomic variability between wild-type and *Hnf4a*$^{+/0}$ mice is reduced in tetraploid hepatocyte nuclei, in both young and old mice (Fig. 4B). Importantly, this transcriptomic buffering in the 4n nuclei from hepatocytes is consistent in all strains of haploinsufficient mice (Fig. 4C). Moreover, early tetraploidisation did not affect the epigenetic clock, indicating that polyploidisation does not accelerate ageing *per se* (Fig. S9). Therefore, early tetraploidisation leads to a transcriptomic buffering in response to a genetic perturbation that is enhanced during ageing.

In order to demonstrate that tetraploid hepatocytes can genetically buffer genomic perturbation through enrichment of the wild-type allele (Figs 4A, S10, and S11), we performed the BaseScope assay, in which a single-pair probe *in-situ* hybridisation was used to detect exon junctions (Fig. 4D, see Methods). Using two uniquely designed ZZ probes to recognise a specific exon junction in the wild-type allele (exon 4 and 5; green) and *Hnf4a*$^{+/0}$ (exon 3 and 6, red), respectively, we quantified cells with different genotypes: *Hnf4a*$^{+/+}$, *Hnf4a*$^{+/0}$, and *Hnf4a*$^{+/0}$, in young and in old mice. We observed a significantly higher number of tetraploid nuclei carrying wild-type alleles in the old hepatocytes, suggesting that early tetraploidisation leads to the non-random segregation of the wild-type allele after genomic perturbation.

Discussion

Why hepatocytes become polyploid, and what mechanisms underlie this transition, has long been debated.[2] Polyploidy has been specifically suggested to buffer genotypic, environmental, and age-related stresses.[8,9] Here, we discovered that haploinsufficiency of any one of three transcription factors triggers early polyploidisation, and, surprisingly, reduced age-associated liver steatosis. These phenotypes were not driven by shared transcriptional perturbations. Instead, increased hepatocyte ploidy appears to be a universal mechanism to cope with genomic perturbations, as haploinsufficiency of either liver regulators (*Hnf4a* or *Cebpa*) or a structural insulator

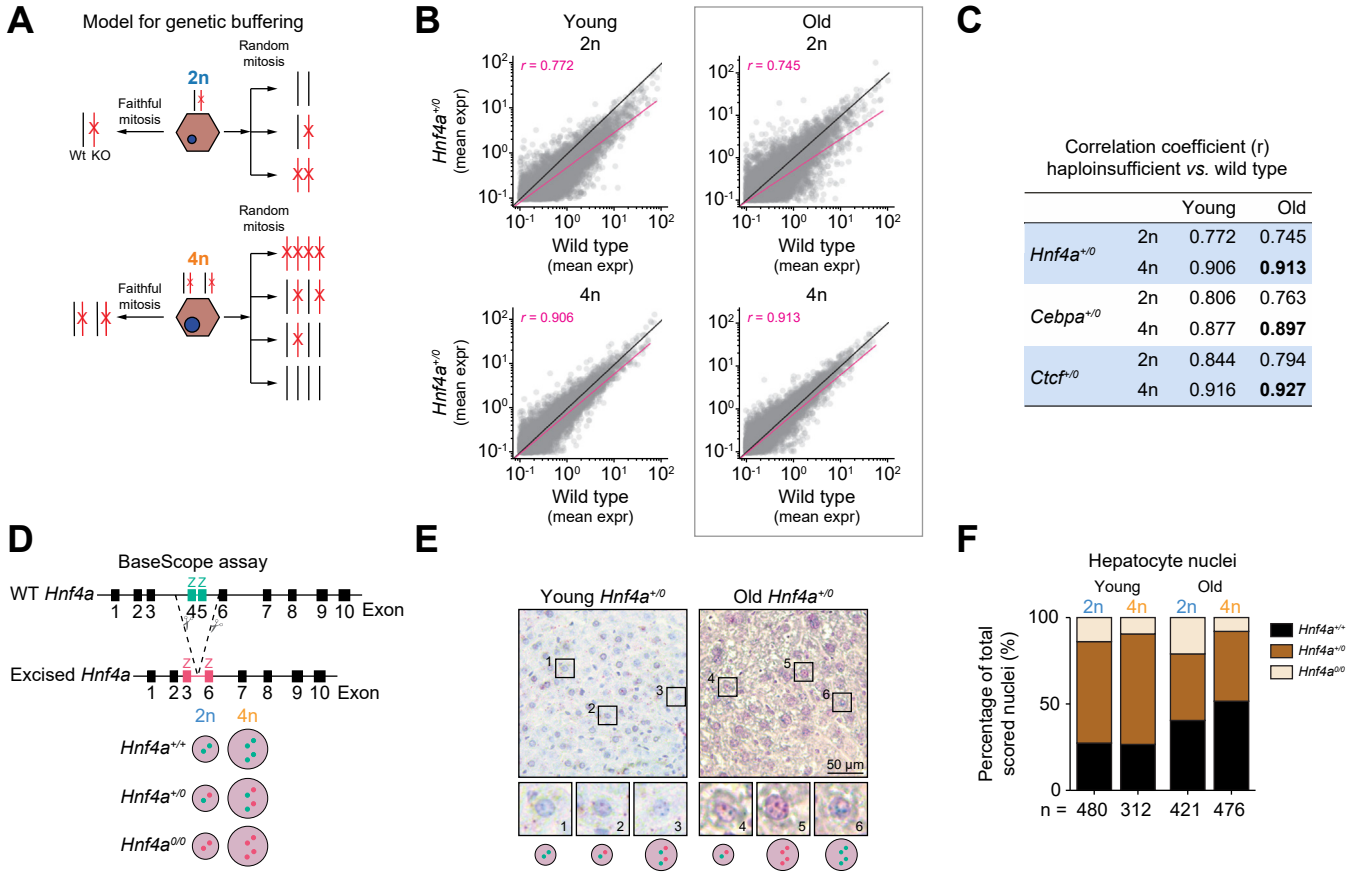

Fig. 4. Enrichment of WT alleles following ageing in polyploid hepatocytes. (A) Early polyploidisation as a mechanism to restore genomic perturbations during ageing. (B) Scatter plot showing correlation analysis of normalised mean gene expression in hepatocytes between WT and *Hnf4a*-haploinsufficient mice by ploidy and age. Black line shows theoretical identity (correlation coefficient of 1.0), magenta line shows empirical correlation (shown as *r*-values per diagram). (C) Correlation coefficient (*r*) of normalised mean gene expression between WT and all haploinsufficient mice by ploidy and age. (D) BaseScope Assay with unique probes for the WT allele (green), and the excised floxed *Hnf4a* allele (red). (E) Representative BaseScope and immunohistochemistry staining of $Hnf4a^{+/0}$ mice (young n = 2, old n = 2; blue: DAPI, green: wild-type, red: excised). (F) Quantification of genotype nuclei from liver sections of two young and two old $Hnf4a^{+/0}$-haploinsufficient mice, categorised as showing WT, hemizygous or complete KO alleles, with total number of quantified nuclei (n) shown on the bottom. KO, knockout; WT, wild-type.

protein (*Ctcf*) leads to similar phenotypic and transcriptional outcomes. Upon ageing, cells containing tetraploid nuclei were enriched for wild-type alleles, suggesting that non-random retention of wild-type alleles during mitosis could be a molecular mechanism to maintain functional homeostasis in the liver.

Our results indicate that diploid and tetraploid hepatocyte nuclei are fundamentally different states, where ploidy conversion is driven by genotypic stress, environmental stress, and/or ageing. Our data revealed that expression of age-related hallmark genes differs dramatically by ploidy, a fact current analyses of liver ageing fail to consider.[44] For instance, *Cyp2e1* is a widely used marker gene transcriptionally increased in aged liver[58,59]; our data revealed that most of this age-related increase is concentrated in tetraploid nuclei; indeed, ploidy-dependence of expression differences was a common phenotype. Furthermore, early tetraploidisation ameliorates age-related fatty liver development in three independent haploinsufficient mice, suggesting that steatosis is not an inevitable result of liver ageing.[47]

Hepatocyte ploidy could be considered a cellular state in which cells make context-aware decisions and adapt to their internal state and external surroundings.[60] Our results further indicate that hepatocyte cell size is primarily determined by ploidy, and may not be a hallmark of ageing in the liver.[61,62] Mechanistically, polyploidisation in the context of both cellular and nuclear ploidy could stoichiometrically buffer transcription by altering the ratio between regulators and their binding sites,[63,64] thus affecting transcriptional bursting and polymerase stalling[50–52,65]. In order to fully understand the role of polyploidy in the liver and its potential clinical implications, longitudinal studies and measurements at intermediate time points will be required to monitor the dynamics of cellular and nuclear ploidy.

Faithful chromosome segregation during ploidy reduction from polyploid to diploid hepatocytes is crucial to regenerate chronically injured livers.[7] Here, we demonstrate that tetraploid nuclei in haploinsufficient mice non-randomly accumulate wild-type alleles, suggesting an underlying mechanism that selectively favours functional alleles and promotes hepatic adaptation. Intriguingly, non-random selection of chromosomes has been observed in $Fah^{-/-}$ mice,[8] and during drug-induced aneuploidy in human cells.[66] We speculate that the non-random selection of wild-type alleles in haploinsufficient mice was facilitated via previously reported mechanisms, including

biased chromosome segregation resting on inter-allelic differences in the concentration of centromeric protein-DNA complexes,[67] or via homologous recombination.[68]

Current single-cell transcriptomic atlases do not consider ploidy,[36,35,45,46,69] despite its widespread occurrence in hepatocytes, cardiomyocytes, osteoclasts, megakaryocytes, trophoblast giant cells, and mammary alveolar cells.[2] Prior studies have shown that tumour suppression is mediated by polyploid hepatocytes.[10,11,49,70,71] Here we have demonstrated the singular importance of polyploidy: in hepatocytes, tetraploid nuclei can act as a distinct cellular state that transcriptionally and genomically buffers phenotypic ageing. Incorporating ploidy as an additional layer of cellular heterogeneity might provide novel insight into functional mechanisms that modulate chronic liver diseases during ageing, including non-alcoholic fatty liver disease, cirrhosis, and hepatocellular carcinoma.

Thus, our results indicate that hepatocyte polyploidy is a general response to genotypic stresses and, unexpectedly, can attenuate age-related changes in transcription and tissue homeostasis.

Affiliations

[1]*Helmholtz Pioneer Campus (HPC), Helmholtz Munich, Neuherberg, Germany;* [2]*Institute of Computational Biology, Computational Health Department, Helmholtz Munich, Neuherberg, Germany;* [3]*Division of Infectious Diseases and Tropical Medicine, Ludwig-Maximilian-Universität Klinikum, Germany;* [4]*Technical University of Munich, Department of Mathematics, 85748 Garching. Munich, Germany;* [5]*German Cancer Research Centre, Heidelberg, Germany;* [6]*German Cancer Research Center, Division of Regulatory Genomics and Cancer Evolution (B270), Heidelberg, Germany;* [7]*Cancer Research UK Cambridge Institute, University of Cambridge, CB20RE, United Kingdom;* [8]*TUM School of Medicine, Technical University of Munich, Munich, Germany;* [9]*Institute of Biotechnology and Biomedicine (BIOTECMED), Department of Biochemistry and Molecular Biology, University of Valencia, Burjassot, Spain*

Abbreviations

HB, homogenisation buffer; PCA, principal component analysis; QC, quality control; STAR, Spliced Transcripts Alignment to a Reference; TPM, transcripts per million; t-SNE, t-distributed stochastic neighbourhood embedding.

Financial support

This research was supported by the Helmholtz Pioneer Campus (K.Y., I.K.D., L.Z., C.P.M-J.), Cancer Research UK (D.T.O. SWAG/051.), Wellcome Trust (D.T.O. 202878/Z/16/Z), ERC (D.T.O. 7883937) the Janet Thornton Fellowship (WT098051 to C.P.M-J.), CIDEGENT program (CIDEXG/2023/30 to C.P.M-J.). The European Association for the Study of the Liver (Andrew K. Burroughs Short-term Training Fellowship to K.Y.), and Helmholtz future topic Ageing and Metabolic Programming (AMPro ZT-0026 to I.K.D).

Conflict of interest

M.B. is currently a full-time employee at Calico LLC.

Please refer to the accompanying ICMJE disclosure forms for further details.

Authors' contributions

K.Y and C.P.M-J. designed experiments; K.Y., I.K.D. M.S. and CP.M-J. performed experiments; M.B., M.S, L.Z., and C.T-L. performed computational analysis. K.Y., M.B., D.T.O., F.T., C.P.M-J interpreted the data; C.P.M-J. designed and aged the haploinsufficient mouse models. K.Y., D.T.O. and C.P.M-J. wrote the manuscript with input from all co-authors. K.Y. and C.P.M-J provided figure editing and design. F.T, D.T.O., C.P.M.J. oversaw the research; All authors commented on and approved the manuscript.

Data availability statement

All raw sequencing data from old and haploinsufficient mice is deposited and publicly available in ArrayExpress/Biostudies under accession number E-MTAB-12738.[77] Raw sequencing data from young wild-type mice was obtained from our previous work deposited in ArrayExpress under accession number E-MTAB-9333.[78] Raw sequencing data from nuclear transcriptome of isolated wild-type hepatocytes with different levels of ploidy during ageing is deposited and publicly available in Biostudies under accession number S-BSST1330.[79] Raw methylation array data during ageing in wild-type and haploinsufficient mice is deposited and publicly available in Biostudies under accession number S-BSST1329[80]

Code availability

The scripts (jupyter notebooks and R code) containing code to reproduce the analysis are publicly available at Github and Zenodo https://github.com/celiamtnez/AgeingKO [81] and https://github.com/celiamtnez/AgingKO2.[82]

Ethics statement

All animal experiments were approved by the UK Home Office regulations, and mice were group-housed under specific pathogen-free conditions under a 12h light/dark cycle in accordance with the University of Cambridge guidelines. Mice had free access to water and to standard mouse chow (PicoLab Mouse Diet 20, 5R58). Cages contained aspen bedding and the following cage enrichments: nesting material, aspen chew stick, and cardboard tunnel. Hemizygous knockout mice ear clipping biopsies were used for genotyping by Transnetyx (Transnetyx). All animal experiments that were carried out in Germany complied with German Animal Welfare Legislation and the regulations of the Government of Upper Bavaria. Animal housing was approved according to §11 of the German Animal Welfare Act and performed in accordance with Directive 2010/63/EU.

Acknowledgements

We are grateful to Dr. Iannis Talianidis and Evangelia C. Tachmatzidi for designing de experiments and providing the liver-specific HNF4A and CEBPA heterozygous knockout samples (Institute of Molecular Biology & Biotechnology, Foundation for Research and Technology Hellas, Heraklion, Crete, Greece). We thank all member of the Martinez-Jimenez laboratory for helpful discussions and all staff (M. Hartman, A. Schröder and A. Barden) of the Helmholtz Pioneer Campus (HPC) at Helmholtz München and Cancer Research UK (CRUK). Specifically, we thank the CRUK-CI core facilities, including Genomics (P. Coupland), Flow Cytometry (J. Markovic-Djuric and R. Grenfell), the Biological Resources Unit (A. Mowbray, N. Jacobs, M. Clayton, and M. Mitchell) for animal husbandry, and the Histopathology/ISH core facility (J. Miller, J. Jones, and C. Brodie). We also thank the Core Genomics at HMGU (I. de la Rosa), HMGU Pathology and Tissue Analytic Core facility (A. Feuchtinger, U. Buchholz, M. Tost and A. Ivanova), the Laboratory Animal Services core facility (J. Zorn, R. Erdelen, D. Würzinger and staff members of E-Streifen), and the Bioinformatics Core (T. Walzthoeni and X. Pastor). We are grateful to all the Core Facilities and staff members for their on-going scientific support and discussions.

Supplementary data

Supplementary data to this article can be found online at https://doi.org/10.1016/j.jhep.2024.03.043.

References

Author names in bold designate shared co-first authorship

[1] **Donne R**, **Saroul-Ainama M**, **Cordier P**, et al. Polyploidy in liver development, homeostasis and disease. Nat Rev Gastroenterol Hepatol 2020;7:391–405.

[2] Sladky VC, Eichin F, Reiberger T, et al. Polyploidy control in hepatic health and disease. J Hepatol 2021;75:1177–1191.

[3] Gentric G, Maillet V, Paradis V, et al. Oxidative stress promotes pathologic polyploidization in nonalcoholic fatty liver disease. J Clin Invest 2015;125:981–992.

[4] Wang MJ, Chen F, Lau JTY, et al. Hepatocyte polyploidization and its association with pathophysiological processes. Cell Death Dis 2017;8:e2805.

[5] Sigal SH, Rajvanshi P, Gorla GR, et al. Partial hepatectomy-induced polyploidy attenuates hepatocyte replication and activates cell aging events. Am J Physiol 1999;276:G1260–G1272.

[6] **Bou-Nader M**, **Caruso S**, **Donne R**, et al. Polyploidy spectrum: a new marker in HCC classification. Gut 2019;2:355–364.

[7] Matsumoto T, Wakefield L, Tarlow BD, et al. In vivo lineage tracing of polyploid hepatocytes reveals extensive proliferation during liver regeneration. Cell Stem Cell 2020;26:34–47 e33.
[8] Duncan AW, Hanlon Newell AE, Bi W, et al. Aneuploidy as a mechanism for stress-induced liver adaptation. J Clin Invest 2012;122:3307–3315.
[9] Duncan AW, Taylor MH, Hickey RD, et al. The ploidy conveyor of mature hepatocytes as a source of genetic variation. Nature 2010;467:707–710.
[10] Diril MK, Ratnacaram CK, Padmakumar VC, et al. Cyclin-dependent kinase 1 (Cdk1) is essential for cell division and suppression of DNA re-replication but not for liver regeneration. Proc Natl Acad Sci U S A 2012;109:3826–3831.
[11] Wilkinson PD, Delgado ER, Alencastro F, et al. The polyploid state restricts hepatocyte proliferation and liver regeneration in mice. Hepatology 2019;69:1242–1258.
[12] Sladky VC, Knapp K, Szabo TG, et al. PIDDosome-induced p53-dependent ploidy restriction facilitates hepatocarcinogenesis. EMBO Rep 2020;21: e50893.
[13] Wilkinson PD, Alencastro F, Delgado ER, et al. Polyploid hepatocytes facilitate adaptation and regeneration to chronic liver injury. Am J Pathol 2019;189:1241–1255.
[14] Margall-Ducos G, Celton-Morizur S, Couton D, et al. Liver tetraploidization is controlled by a new process of incomplete cytokinesis. J Cel Sci 2007;120:3633–3639.
[15] Hayhurst GP, Lee YH, Lambert G, et al. Hepatocyte nuclear factor 4alpha (nuclear receptor 2A1) is essential for maintenance of hepatic gene expression and lipid homeostasis. Mol Cel Biol 2001;21:1393–1403.
[16] Odom DT, Zizlsperger N, Gordon DB, et al. Control of pancreas and liver gene expression by HNF transcription factors. Science 2004;303: 1378–1381.
[17] Ballester B, Medina-Rivera A, Schmidt D, et al. Multi-species, multi-transcription factor binding highlights conserved control of tissue-specific biological pathways. Elife 2014;3:e02626.
[18] Nishikawa T, Bell A, Brooks JM, et al. Resetting the transcription factor network reverses terminal chronic hepatic failure. J Clin Invest 2015;125: 1533–1544.
[19] Schmidt D, Wilson MD, Ballester B, et al. Five-vertebrate ChIP-seq reveals the evolutionary dynamics of transcription factor binding. Science 2010;328: 1036–1040.
[20] Martinez-Jimenez CP, Kyrmizi I, Cardot P, et al. Hepatocyte nuclear factor 4alpha coordinates a transcription factor network regulating hepatic fatty acid metabolism. Mol Cel Biol 2010;30:565–577.
[21] Matsuo S, Ogawa M, Muckenthaler MU, et al. Hepatocyte nuclear factor 4alpha controls iron metabolism and regulates transferrin receptor 2 in mouse liver. J Biol Chem 2015;290:30855–30865.
[22] Lee YH, Sauer B, Johnson PF, et al. Disruption of the c/ebp alpha gene in adult mouse liver. Mol Cel Biol 1997;17:6014–6022.
[23] Shih DQ, Heimesaat M, Kuwajima S, et al. Profound defects in pancreatic beta-cell function in mice with combined heterozygous mutations in Pdx-1, Hnf-1alpha, and Hnf-3beta. Proc Natl Acad Sci U S A 2002;99:3818–3823.
[24] Shih DQ, Dansky HM, Fleisher M, et al. Genotype/phenotype relationships in HNF-4alpha/MODY1: haploinsufficiency is associated with reduced apolipoprotein (AII), apolipoprotein (CIII), lipoprotein(a), and triglyceride levels. Diabetes 2000;49:832–837.
[25] Boj SF, Petrov D, Ferrer J. Epistasis of transcriptomes reveals synergism between transcriptional activators Hnf1alpha and Hnf4alpha. Plos Genet 2010;6:e1000970.
[26] Ng NHJ, Jasmen JB, Lim CS, et al. HNF4A haploinsufficiency in MODY1 abrogates liver and pancreas differentiation from patient-derived induced pluripotent stem cells. iScience 2019;16:192–205.
[27] Stoffel M, Duncan SA. The maturity-onset diabetes of the young (MODY1) transcription factor HNF4alpha regulates expression of genes required for glucose transport and metabolism. Proc Natl Acad Sci U S A 1997;94: 13209–13214.
[28] Moore JM, Rabaia NA, Smith LE, et al. Loss of maternal CTCF is associated with peri-implantation lethality of Ctcf null embryos. PLoS One 2012;7:e34915.
[29] Choi Y, Song MJ, Jung WJ, et al. Liver-specific deletion of mouse CTCF leads to hepatic steatosis via augmented PPARgamma signaling. Cell Mol Gastroenterol Hepatol 2021;12:1761–1787.
[30] Aitken SJ, Ibarra-Soria X, Kentepozidou E, et al. CTCF maintains regulatory homeostasis of cancer pathways. Genome Biol 2018;19:106.
[31] Kemp CJ, Moore JM, Moser R, et al. CTCF haploinsufficiency destabilizes DNA methylation and predisposes to cancer. Cell Rep 2014;7:1020–1029.
[32] Hunt NJ, Kang SWS, Lockwood GP, et al. Hallmarks of aging in the liver. Comput Struct Biotechnol J 2019;17:1151–1161.
[33] Finan B, Clemmensen C, Zhu Z, et al. Chemical hybridization of glucagon and thyroid hormone optimizes therapeutic impact for metabolic disease. Cell 2016;167:843–857 e814.
[34] Riordan JD, Nadeau JH. Modeling progressive non-alcoholic fatty liver disease in the laboratory mouse. Mamm Genome 2014;25:473–486.
[35] **Richter ML**, **Deligiannis IK**, Yin K, et al. Single-nucleus RNA-seq2 reveals functional crosstalk between liver zonation and ploidy. Nat Commun 2021;12:4264.
[36] Tabula Muris C. A single-cell transcriptomic atlas characterizes ageing tissues in the mouse. Nature 2020;583:590–595.
[37] Chen HC, **Eling N**, **Martinez-Jimenez CP**, et al. IL-7-dependent compositional changes within the gammadelta T cell pool in lymph nodes during ageing lead to an unbalanced anti-tumour response. EMBO Rep 2019;20:e47379.
[38] **Martinez-Jimenez CP**, **Eling N**, Chen HC, et al. Aging increases cell-to-cell transcriptional variability upon immune stimulation. Science 2017;355: 1433–1436.
[39] Marti GEW, Chu S, Quake SR. Aging causes changes in transcriptional noise across a diverse set of cell types. bioRxiv 2022. 2022.2006.2023.497402.
[40] Enge M, Arda HE, Mignardi M, et al. Single-cell analysis of human pancreas reveals transcriptional signatures of aging and somatic mutation patterns. Cell 2017;171:321–330 e314.
[41] Tanami S, Ben-Moshe S, Elkayam A, et al. Dynamic zonation of liver polyploidy. Cell Tissue Res 2017;368:405–410.
[42] Chondronasiou D, Gill D, Mosteiro L, et al. Multi-omic rejuvenation of naturally aged tissues by a single cycle of transient reprogramming. Aging Cell 2022;21:e13578.
[43] Zhang MJ, Pisco AO, Darmanis S, et al. Mouse aging cell atlas analysis reveals global and cell type-specific aging signatures. Elife 2021;10.
[44] White RR, Milholland B, MacRae SL, et al. Comprehensive transcriptional landscape of aging mouse liver. BMC Genomics 2015;16:899.
[45] **Palovics R**, **Keller A**, **Schaum N**, et al. Molecular hallmarks of heterochronic parabiosis at single-cell resolution. Nature 2022;603:309–314.
[46] Ma S, Wang S, Ye Y, et al. Heterochronic parabiosis induces stem cell revitalization and systemic rejuvenation across aged tissues. Cell Stem Cell 2022;29:990–1005 e1010.
[47] Ogrodnik M, Miwa S, Tchkonia T, et al. Cellular senescence drives age-dependent hepatic steatosis. Nat Commun 2017;8:15691.
[48] Kyrmizi I, Hatzis P, Katrakili N, et al. Plasticity and expanding complexity of the hepatic transcription factor network during liver development. Genes Dev 2006;20:2293–2305.
[49] Matsumoto T, Wakefield L, Peters A, et al. Proliferative polyploid cells give rise to tumors via ploidy reduction. Nat Commun 2021;12:646.
[50] Bartman CR, Hamagami N, Keller CA, et al. Transcriptional burst initiation and polymerase pause release are key control points of transcriptional regulation. Mol Cel 2019;73:519–532 e514.
[51] Stavreva DA, Garcia DA, Fettweis G, et al. Transcriptional bursting and Co-bursting regulation by steroid hormone release pattern and transcription factor mobility. Mol Cel 2019;75:1161–1177 e1111.
[52] Bozukova M, Nikopoulou C, Kleinenkuhnen N, et al. Aging is associated with increased chromatin accessibility and reduced polymerase pausing in liver. Mol Syst Biol 2022;18:e11002.
[53] Wang DC, Wang X. Clinical significance of spatiotemporal transcriptional bursting and control. Clin Transl Med 2021;11:e518.
[54] **Zhang X**, **Li S**, **Zhou Y**, et al. Ablation of cytochrome P450 omega-hydroxylase 4A14 gene attenuates hepatic steatosis and fibrosis. Proc Natl Acad Sci U S A 2017;114:3181–3185.
[55] Moon YA, Hammer RE, Horton JD. Deletion of ELOVL5 leads to fatty liver through activation of SREBP-1c in mice. J Lipid Res 2009;50:412–423.
[56] Miettinen TP, Pessa HK, Caldez MJ, et al. Identification of transcriptional and metabolic programs related to mammalian cell size. Curr Biol 2014;24: 598–608.
[57] Kreutz C, MacNelly S, Follo M, et al. Hepatocyte ploidy is a diversity factor for liver homeostasis. Front Physiol 2017;8:862.
[58] Wauthier V, Verbeeck RK, Calderon PB. The effect of ageing on cytochrome p450 enzymes: consequences for drug biotransformation in the elderly. Curr Med Chem 2007;14:745–757.
[59] Abdelmegeed MA, Choi Y, Ha SK, et al. Cytochrome P450-2E1 promotes aging-related hepatic steatosis, apoptosis and fibrosis through increased nitroxidative stress. Free Radic Biol Med 2016;91:188–202.
[60] Kramer BA, Sarabia Del Castillo J, Pelkmans L. Multimodal perception links cellular state to decision-making in single cells. Science 2022;377:642–648.
[61] Lengefeld J, Cheng CW, Maretich P, et al. Cell size is a determinant of stem cell potential during aging. Sci Adv 2021;7:eabk0271.

[62] Lanz MC, Zatulovskiy E, Swaffer MP, et al. Increasing cell size remodels the proteome and promotes senescence. Mol Cel 2022;82:3255–3269 e3258.
[63] Lundgren M, Chow CM, Sabbattini P, et al. Transcription factor dosage affects changes in higher order chromatin structure associated with activation of a heterochromatic gene. Cell 2000;103:733–743.
[64] Padovan-Merhar O, Nair GP, Biaesch AG, et al. Single mammalian cells compensate for differences in cellular volume and DNA copy number through independent global transcriptional mechanisms. Mol Cel 2015;58:339–352.
[65] **Gyenis A**, **Chang J**, Demmers J, et al. Genome-wide RNA polymerase stalling shapes the transcriptome during aging. Nat Genet 2023;55:268–279.
[66] Worrall JT, Tamura N, Mazzagatti A, et al. Non-random mis-segregation of human chromosomes. Cel Rep 2018;23:3366–3380.
[67] Dumont M, Gamba R, Gestraud P, et al. Human chromosome-specific aneuploidy is influenced by DNA-dependent centromeric features. EMBO J 2020;39:e102924.
[68] **Ouyang J**, **Yadav T**, Zhang JM, et al. RNA transcripts stimulate homologous recombination by forming DR-loops. Nature 2021;594:283–288.
[69] **Katsuda T**, **Hosaka K**, Matsuzaki J, et al. Transcriptomic dissection of hepatocyte heterogeneity: linking ploidy, zonation, and stem/progenitor cell characteristics. Cel Mol Gastroenterol Hepatol 2020;9:161–183.
[70] Zhang S, Zhou K, Luo X, et al. The polyploid state plays a tumor-suppressive role in the liver. Dev Cel 2018;44:447–459 e445.
[71] Zhang S, Nguyen LH, Zhou K, et al. Knockdown of anillin actin binding protein blocks cytokinesis in hepatocytes and reduces liver tumor development in mice without affecting regeneration. Gastroenterology 2018;154:1421–1434.
[72] Strzelecki M, Yin K, Talavera-Lopez C, et al. Isolation of nuclei from flash-frozen liver tissue for single-cell multiomics. J Vis Exp 2022:190.
[73] Canchola JA, Tang S, Hemyari P, et al. Correct use of percent coefficient of variation (%CV) formula for log-transformed data. MOJ Proteomics & Bioinformatics 2017;6:316–317.
[74] **Halpern KB**, **Shenhav R**, Matcovitch-Natan O, et al. Single-cell spatial reconstruction reveals global division of labour in the mammalian liver. Nature 2017;542:352–356.
[75] Haghverdi L, Buettner F, Theis FJ. Diffusion maps for high-dimensional single-cell analysis of differentiation data. Bioinformatics 2015;31:2989–2998.
[76] Zhou W, Triche Jr TJ, Laird PW, et al. SeSAMe: reducing artifactual detection of DNA methylation by Infinium BeadChips in genomic deletions. Nucleic Acids Res 2018;46:e123.
[77] **Yin K**, **Büttner M**, Deligiannis IK, et al. Hepatocyte polyploidization during ageing protects against transcriptional dysregulation and chronic liver disease. ArrayExpress/Biostudies; 2023. E-MTAB-12738, https://www.ebi.ac.uk/biostudies/studies/E-MTAB-12738.
[78] Deligiannis IK, Martinez-Jimenez C. Single-nucleus RNA-seq2 of liver tissue of 3 months old mice to investigate crosstalk between ploidy and zonation. ArrayExpress/BioStudies 2021. E-MTAB-9333, https://www.ebi.ac.uk/biostudies/arrayexpress/studies/E-MTAB-9333.
[79] **Yin K**, **Büttner M**, Deligiannis IK, et al. snRNA-seq analysis of the nuclear transcriptome of hepatocytes with different levels of ploidy during ageing in wild-type mice. BioStudies, S-BSST1330 2023. https://www.ebi.ac.uk/biostudies/studies/S-BSST1330.
[80] **Yin K**, **Büttner M**, Deligiannis IK, et al. Analysis of the epigenetic clock in liver tissue from young and old mice of different strains (C57BL6/J, Hnf4a+/0, Cebpa+/0, and Ctcf +/0). Biostudies 2023. S-BSST1329, https://www.ebi.ac.uk/biostudies/studies/S-BSST1329.
[81] **Yin K**, **Büttner M**, Deligiannis IK, et al. Polyploidisation pleiotropically buffers ageing in hepatocytes. AgingKO. Zenodo; 2023. https://doi.org/10.5281/zenodo.10598490.
[82] **Yin K**, **Büttner M**, Deligiannis IK, et al. Polyploidisation pleiotropically buffers ageing in hepatocytes. AgingKO2. Zenodo; 2023. https://doi.org/10.5281/zenodo.10598370.